Effect of different types of damping winding structures on the no-load magnetic field of a tubular hydro-generator

QIAO-YUN ZHENG¹, ZHEN-NAN FAN^{1,2*}, ZHI-TING ZHOU²

¹The Key Laboratory of Fluid and Power Machinery, Ministry of Education, Xihua University Chengdu, 610039, China

²State Key Laboratory of Power Transmission Equipment & System security and New Technology Chongqing University Chongqing, 400030, China

e-mail: {*fanzhennan/dianyingcc}@126.com, 2839793947@qq.com

Abstract: The no-load magnetic field of a hydro-generator significantly impacts the quality of its no-load voltage waveform and the grid power quality and power system stability. As a vital element for ensuring the safe and steady operation of hydrogenerators, the damping winding structure directly affects the state of the no-load magnetic field. Particularly, horizontal hydro-generators, such as tubular turbine units, feature confined and irregular internal spaces that lead to more intricate and intense distributions of the magnetic field. Therefore, to improve the quality of noload voltage waveforms, grid power quality, and overall power system stability, it is essential to examine how variations in damping winding structure types affect the no-load magnetic field in these generators. This paper considers a specific 34-MW large tubular turbine generator as an example. A 2D transient electromagnetic field model was developed to investigate the effects of four damping winding structures fully damped, semi-damped, isolated damping bar, and solid-steel pole—on the magnitude and distribution of the no-load magnetic field, the quality of the no-load voltage waveforms, and the eddy-current losses within the damping system. The research directly supports the design and manufacturing processes of tubular hydro-generators and ensures the safety and stability of generator and power system operations.

Key words: damping winding structure, no-load magnetic field, power quality, tubular hydro-generator

1. Introduction

The no-load magnetic field in a hydro-generator significantly influences the quality of the no-load voltage waveform and has implications for grid power quality and power system stability. The type of damping winding structure is a critical factor that impacts the generator's no-load magnetic field state, ensuring safe and stable operation. In horizontal

tubular hydro-generators, designed to satisfy performance standards such as low head, high flow capacity, and hydraulic efficiency, the challenge lies in effectively arranging turbine and generator components within a constrained internal space. This compact configuration, depicted in Fig. 1, diverges from traditional vertical designs and results in complex distributions and dynamics of the no-load magnetic field within the limited, irregular internal space. Thus, it is crucial to investigate how different types of damping winding structures affect the no-load magnetic field in these generators. This research aims to optimize the magnetic field configuration to ensure the generation of high-quality no-load voltage waveforms, which will subsequently enhance grid power quality and strengthen power system stability.

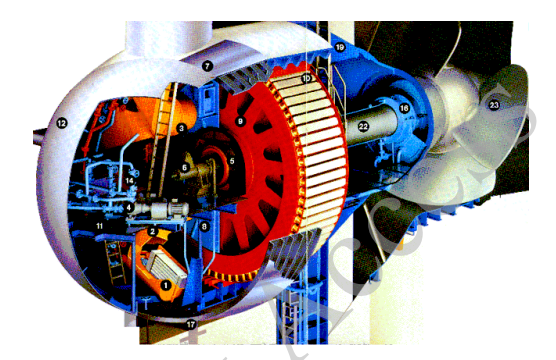


Fig. 1. Tubular hydro-generator structure

Hydro-generator damping winding structures can generally be categorized into four types, as outlined in Table 1. The two most common configurations are the fully damped and semi-damped structures [1–2]. In the fully damped structure, all magnetic pole dampers are interconnected via end rings, forming a short-circuit arrangement where the damping windings of each pole are linked together, creating a cage-like formation, as illustrated in Fig. 2(a). Conversely, the semi-damped structure does not connect the damping windings between the poles, allowing each magnetic pole's damping winding to function independently and be self-contained, as depicted in Fig. 2(b). Additionally, there are two less common configurations: the isolated damping bar arrangement, which features damping bars that are not interconnected, as shown in Fig. 2(c), and the solid-steel pole arrangement that employs monolithic steel poles without dedicated damping windings, as illustrated in Fig. 2(d).

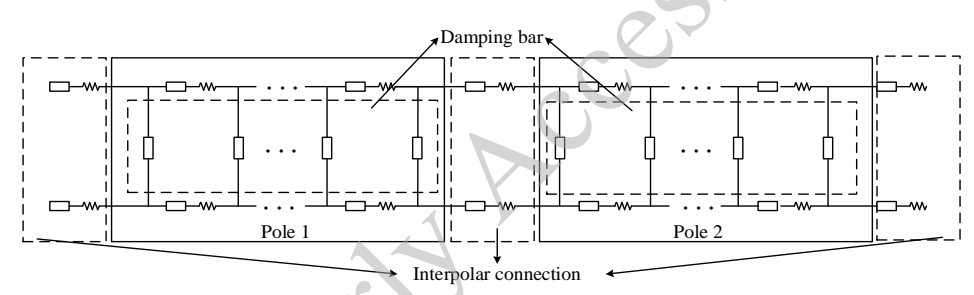
Although substantial research has been conducted on the no-load magnetic field and voltage waveforms of hydro-generators [3–22], the majority of existing studies focus on specific localized structural parameters, such as the skewed stator slot [11–15], the offset of the magnetic pole boot center, the damping bar center offset [16–19], and the damping winding pitch size [20–22] regarding their impact on these characteristics. In contrast, there is a paucity of literature that systematically examines the effects of fundamental damping winding structure types (e.g., fully damped, semi-damped, isolated damping bar, and solid-steel poles) on the no-load magnetic field and voltage waveform quality of tubular hydro-generators.

This paper examines a specific 34 MW tubular hydro-generator. By creating a 2D transient electromagnetic field finite element analysis model, the study explores how four typical damping

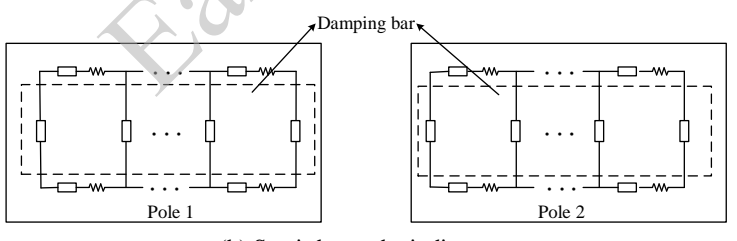
winding structures—fully damped, semi-damped, isolated damping, and solid-steel pole—affect the magnitude and distribution of the no-load magnetic field, the quality of the no-load voltage waveform, and the eddy-current losses in the damping system. The findings provide direct support for improving the design and manufacturing standards of cross-flow hydro-generators, thereby contributing to the stability of power systems.

Table 1. Damping winding structure schemes

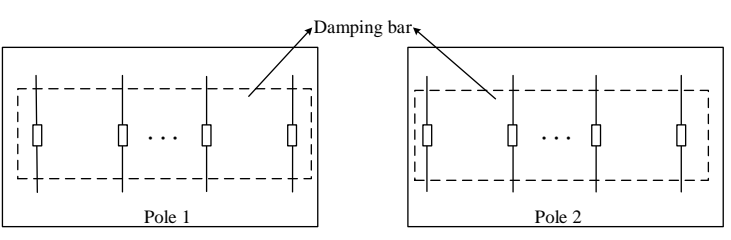
Scheme	Structural description	
1	Fully damped winding structure	
2	Semi-damped winding structure	
3	Isolated damping bar structure	
4	Solid-steel pole structure	



(a) Fully damped winding structure



(b) Semi-damped winding structure



(c) Isolated damping bar structure



(d) Solid-steel pole structure Fig. 2. Schematic diagram of the design scheme of the damping winding structure

2. Modeling of tubular hydro-generator

2.1. Generator basic parameters

This research utilizes a 2D model of a specific 34 MW tubular hydro-generator operating under no-load conditions. Key parameters for the model are shown in Table 2.

Table 2. Key parameters of the tubular hydro-generator

Parameter	Value
Rated power (MW)	34
Rated voltage (kV)	10.5
Power factor	0.95
Number of phases	3
Number of poles	44
Number of slots per phase per pole	2
No-load excitation current (A)	547
Number of damping bars per pole	6
Stator inner diameter (mm)	5 620
Stator outer diameter (mm)	6 0 2 0
Rotor inner diameter (mm)	4 690
Rotor outer diameter (mm)	5 610
Minimal air gap (mm)	10
Maximum-to-minimum air gap ratio	≈1.5
Pole shoe width (mm)	265
Pole body width (mm)	175
Stator slot width (mm)	28
Number of turns of excitation winding	18

2.2. Motion electromagnetic field boundary problem for generators

A range of magnetic poles is selected as the 2D electromagnetic field solution region for the generator, as illustrated in Fig. 3.

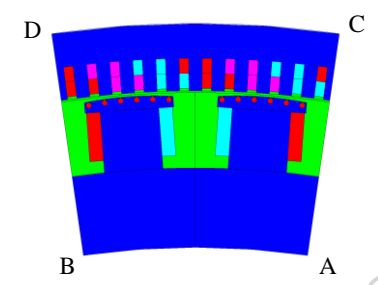


Fig. 3. Generator two-dimensional electromagnetic field solution domain

In the 2D model, it is assumed that the current density and vector magnetic potential only have components along the *z*-axis. In contrast, the velocity has components solely along the *x*-axis. By applying the Coulomb norm $\nabla \cdot \mathbf{A} = 0$ and incorporating boundary conditions, the boundary value problem for the 2D nonlinear time-varying motion electromagnetic field of the generator can be formulated:

Indiated:
$$\begin{cases}
\frac{\partial}{\partial x} \left(v \frac{\partial A_z}{\partial x} \right) + \frac{\partial}{\partial y} \left(v \frac{\partial A_z}{\partial y} \right) = -J_{sz} + \sigma \frac{\partial A_z}{\partial t} + V_x \sigma \frac{\partial A_z}{\partial x} \\
A_z|_{AB} = A_z|_{CD} = 0
\end{cases}, \tag{1}$$

where A represents the vector magnetic potential; J_{SZ} denotes the z-axis component of the externally induced source current density; v indicates the magnetoresistivity of the medium; V signifies the velocity of the medium with respect to the reference coordinate system; and σ stands for the conductivity of the medium.

Based on this, the circuit law is applied to establish the circuit equations for both the generator stator and rotor (including damping windings), which are then integrated with the generator electromagnetic field boundary value problem equations. The time-step finite element method is employed to solve for the no-load magnetic field and no-load voltage waveforms through spatial and temporal discretization.

2.3. Generator no-load voltage harmonics related parameters

The voltage total harmonic distortion (THD) is employed to measure the extent to which harmonic sources cause the actual line voltage waveform to deviate from a sinusoidal form. According to the latest Chinese national standard GB/T 1029-2021, its value is determined by Eq. (2).

THD =
$$\frac{\sqrt{U_2^2 + U_3^2 + \dots + U_n^2}}{U_1} \times 100\%$$
. (2)

In the previous Chinese national standard GB/T 1029-2005 and several other international standards, the telephone harmonic factor (THF) is specified to more precisely assess the degree of disturbance caused by the generator's no-load voltage harmonic component on communication lines, with its value given by Eq. (3).

THF =
$$\frac{\sqrt{U_1^2 \lambda_1^2 + U_2^2 \lambda_2^2 + \dots + U_n^2 \lambda_n^2}}{U} \times 100\%,$$
 (3)

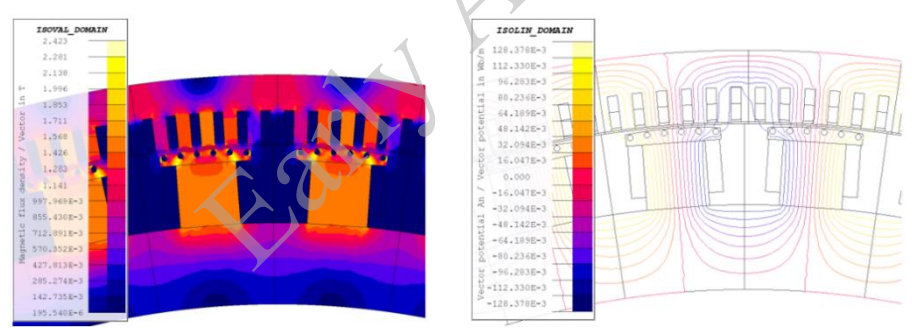
where U represents the root mean square (RMS) value of the line voltage; U_n indicates the RMS value of the n-th harmonic in the line voltage; and λ_n embodies the impact of the n-th harmonic on the telecommunication line.

To comply with grid power quality standards and ensure the stability of power systems, the electrical machine design and manufacturing industry typically requires that large generators meet the criteria of THD \leq 5% and THF \leq 1.5%.

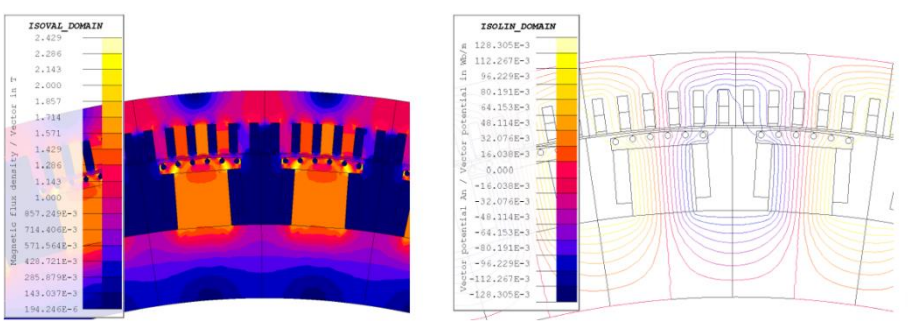
3. Comparative analysis of calculation results

3.1. Generator magnetic field

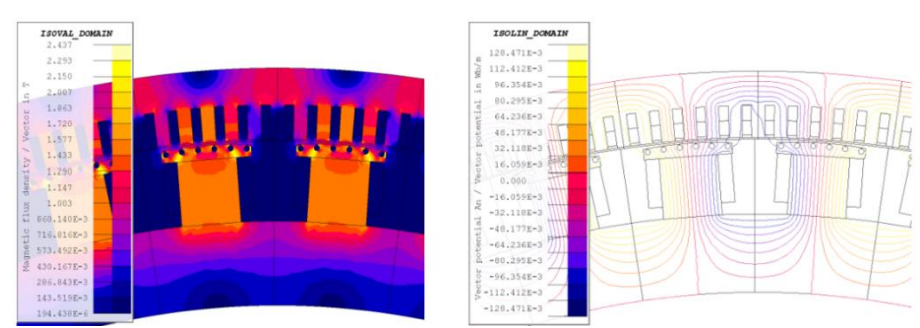
The distributions of the magnetic field corresponding to the four types of damping winding structures are presented in Fig. 4, with relevant data summarized in Table 3.



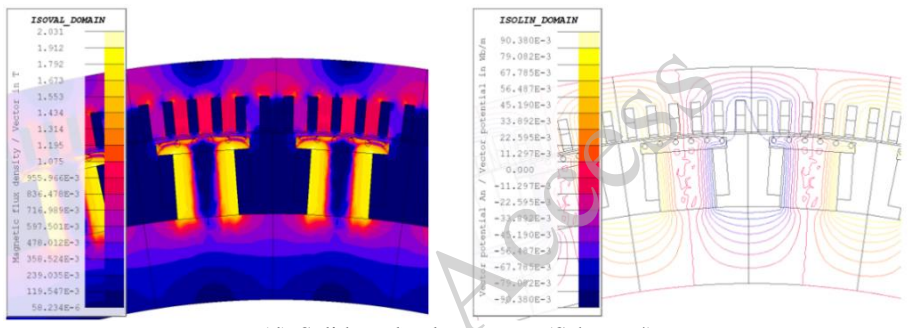
(a) Fully damped winding structure (Scheme 1)



(b) Semi-damped winding structure (Scheme 2)



(c) Isolated damping bar structure (Scheme 3)



(d) Solid-steel pole structure (Scheme 4)

Fig. 4. Magnetic field distribution corresponding to four damping winding structures

Table 3. Comparison of magnetic field distribution values

Scheme	Magnetic flux density (T)		Vector magnetic potential (Wb/m)	
	Minimum	Maximum	Minimum	Maximum
1	0.000195	2.423	-0.128378	0.128378
2	0.000194	2.429	-0.128305	0.128305
3	0.000194	2.437	-0.128471	0.128471
4	0.000058	2.031	-0.090380	0.090380

The air-gap flux density distribution associated with the four types of damping winding structures is displayed in Fig. 5 (one pole region):

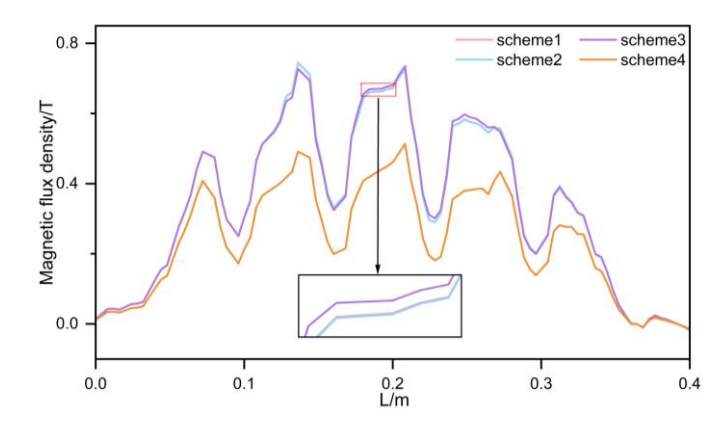


Fig. 5. Comparison of air-gap flux density distribution corresponding to one pole of four damping winding structures

As can be seen from the above graphs:

- 1) The distributions of the magnetic field, magnetic flux density values, vector magnetic potential values, and air-gap flux density waveforms for structures with fully damped (Scheme 1), semi-damped (Scheme 2), and isolated damping bars (Scheme 3) are similar. Specifically, the parameters for fully damped and semi-damped structures show a high degree of consistency. In contrast, the values for magnetic flux density and vector magnetic potential in the isolated damping bar structure are slightly higher than those in the previous two cases, and the air-gap flux density waveforms also exhibit minor differences.
- 2) The magnetic field distributions in the solid-steel pole structure (Scheme 4) show substantial differences compared to the previously mentioned three damping winding structures. Especially notable is the uneven magnetic field distribution in the solid-steel pole structure, which exhibits a significant skin effect; here, the magnetic flux density near the pole's surface is much greater than in other areas of the pole. At the same time, the corresponding values for magnetic flux density, vector magnetic potential, and amplitudes of air-gap flux density waveforms are significantly lower than those of the three damping winding structures.

3.2. No-load RMS voltage

The calculations for the no-load RMS voltage are presented in Table 4.

Scheme Calculated value (V) Designed value (V) **Deviation** 1 10511.8 10500 0.1123% 2 10503.5 10500 0.0333% 3 10540.6 10500 0.3867% 4 7218.1 10500 31.26%

Table 4. Calculation results of the no-load voltage RMS

From Table 4, it is evident that:

When employing fully damped, semi-damped, and isolated damping bar structures, the differences in no-load RMS voltage are relatively minor and closely align with the design value. However, with the solid-steel pole structure, there is a marked difference in results compared to the first three structures. The calculations in Table 4 indicate that the deviation between the calculated value and the design value reaches 31.26%, which is unacceptable.

This discrepancy can be traced back to the magnetic field analysis results. For the fully damped, semi-damped, and isolated damping bar structures, the no-load magnetic field analysis results are very similar. Conversely, the magnetic flux density values, vector magnetic potential values, and amplitudes of air-gap flux density waveforms for the solid-steel pole structure are considerably less than those of the other three damping winding structures. This significant difference results in a considerable deviation between the calculated no-load voltage value and the design value.

3.3. No-load voltage waveform

The no-load voltage waveform (including its amplitude spectrum) and its quality parameters (THD and THF) are calculated and illustrated in Fig. 6 and Fig. 7.

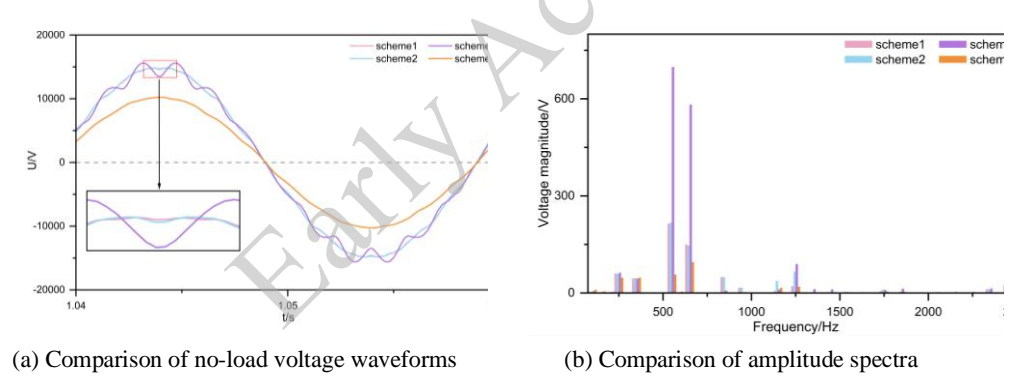


Fig. 6. Comparison of no-load voltage waveforms and amplitude spectra of the output of four damping winding structures

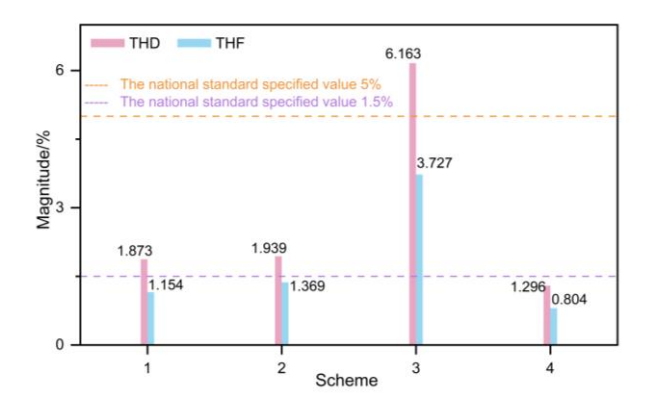


Fig. 7. THD and THF calculation results

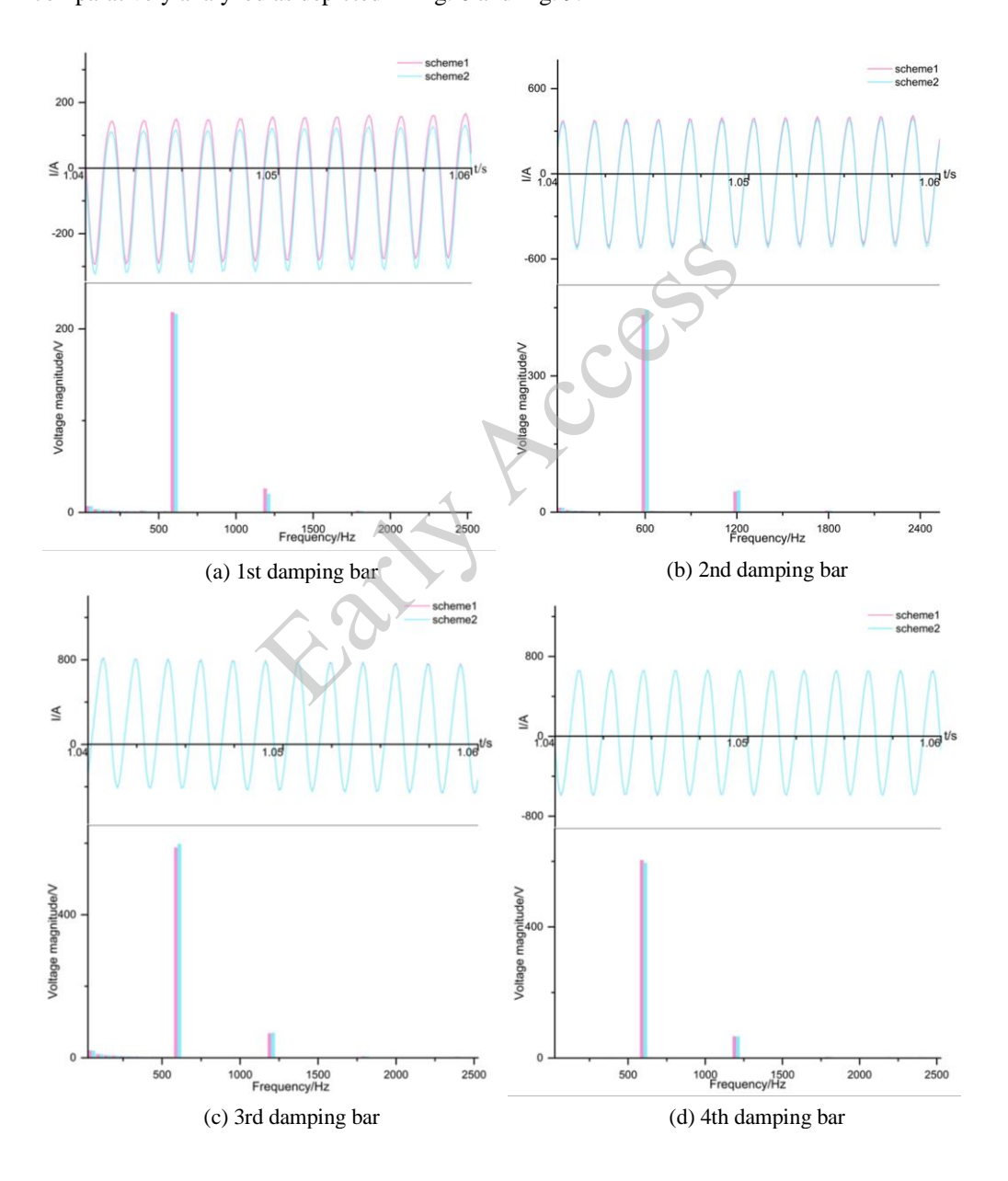
From Fig. 6 and Fig. 7, it can be observed:

- 1) The no-load voltage waveform and its quality parameters align closely when using fully damped and semi-damped structures; in fact, the no-load voltage waveforms of these two structures are nearly indistinguishable. However, the THD and THF parameters calculated for the fully damped structure are lower than those of the semi-damped structure. As a consequence, the no-load voltage waveforms of the fully damped windings are closer to a sinusoidal form, resulting in less interference with communication lines, thus demonstrating superior quality in the no-load voltage waveform from the fully damped structures.
- 2) In the case of the isolated damping winding structure, significant fluctuations occur in the no-load voltage waveform, with the quality parameters THD and THF showing noticeably larger values, which do not meet the industrial standards of THD \leq 5% and THF \leq 1.5%.
- 3) When utilizing the solid-steel pole structure, the amplitude of the no-load voltage waveform markedly decreases compared to other structures. Nevertheless, the quality parameters THD and THF for the no-load voltage waveform are the most favorable among the four damping winding structures.
- 4) In the no-load voltage amplitude spectrum, the harmonic amplitudes exhibit only minor differences between the fully damped and semi-damped configurations across frequencies, while the isolated damping bar configuration yields the highest amplitudes and the solid-steel pole yields the lowest. These characteristic harmonic amplitude variations consistently correlate with the distinct waveform features manifested in each case.

According to electromagnetic induction principles, the no-load voltage waveform of a generator arises from the magnetic field in the stator winding. Specifically, the generator's no-load magnetic field is a composite field formed through the interaction of two components: the primary magnetic field generated by the excitation current and the supplementary magnetic field produced by the currents in the damping windings. Notably, since the excitation winding current and the number of turns are consistent across the four damping winding configurations, their corresponding magnetomotive forces are uniform as well. Therefore, variations in the damping bar currents and the resulting additional magnetic fields are likely key factors that affect differences in the generator's no-load magnetic field—and consequently, its no-load voltage waveform.

Therefore, to clarify the reasons behind the variations in the no-load voltage calculation results mentioned above, it is imperative to examine the damping winding currents (or related losses) associated with different damping winding structures.

The currents in the damping bars of fully damped and semi-damped winding structures are comparatively analyzed as depicted in Fig. 8 and Fig. 9.



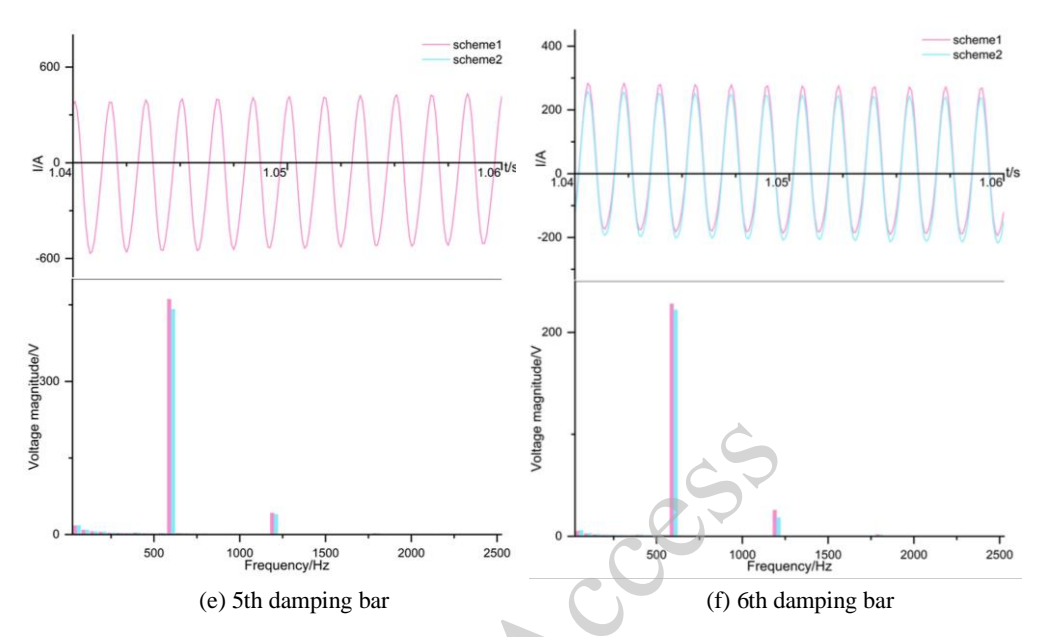


Fig. 8. Comparison of current waveforms and amplitude spectra between fully damped and semi-damped winding structures with 1–6 damping bars

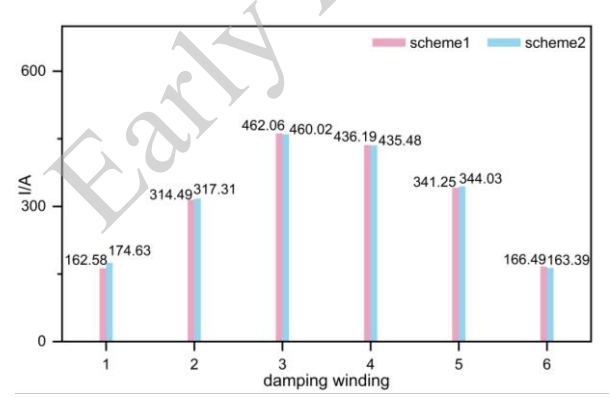


Fig. 9. Comparison of current RMS values of 1–6 damping bars for fully damped and semi-damped winding structures

From the figures, it can be observed that the current waveforms of damping bars 2 to 5 per magnetic pole show nearly identical shapes between the fully and semi-damped windings, with comparable RMS values. The significant differences in waveform and RMS values occur only in the first and sixth bars. The harmonic amplitudes at different frequencies are also very close, reflecting the slight differences in the current waveforms of the damping windings in fully damped and semi-damped structures. As a result, the additional magnetic fields generated by both fully damped and semi-damped windings demonstrate negligible differences.

Consequently, their no-load magnetic fields are highly akin, leading to nearly overlapping no-load voltage waveforms generated in the stator windings.

Electrically isolated damping bars create incomplete current paths, limiting eddy currents to localized circulation within individual bars, resulting in minimal (approaching zero) eddy currents contained within the damping bars themselves. This characteristic is supported by the comparative graphs of eddy-current losses for the three configurations (see Fig. 10). Thus, compared to fully damped and semi-damped structures, the additional magnetic fields induced by the current in the damping bars of the isolated damping winding structure exhibit significantly reduced coupling with the main field (as illustrated in Fig. 5). This leads to a relatively diminished contribution to enhancing both the main field and the quality of the noload voltage waveform. As shown in Fig. 6, this results in poorer quality no-load voltage waveforms in comparison to the other configurations.

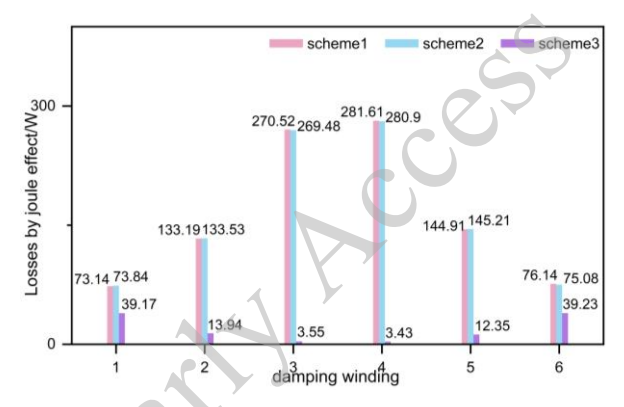
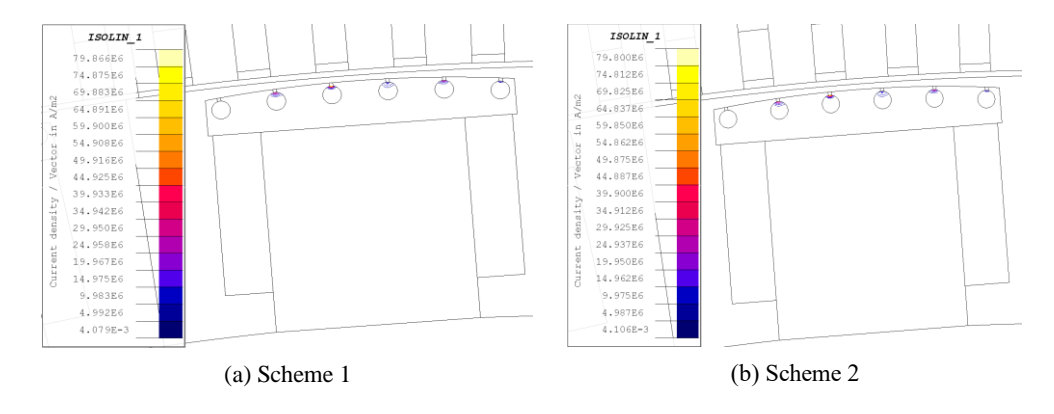


Fig. 10. Comparison of eddy-current losses for fully damped, semi-damped, and isolated damping winding structures with 1–6 damping bars

By employing the previously mentioned methodology, a comparative analysis was conducted to evaluate the rotor pole face eddy-current losses related to the four damping winding configurations, as illustrated in Fig. 11, and summarized in Table 5.



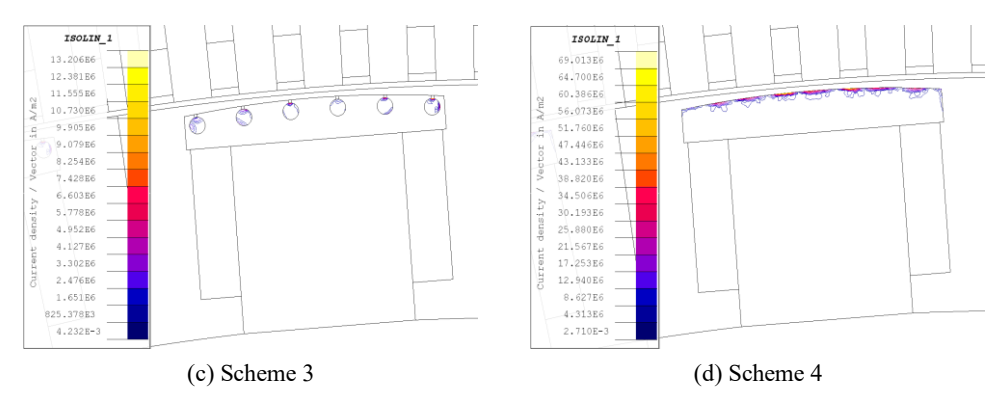


Fig. 11. Rotor pole face eddy-current density for four damping winding configurations

Table 5. Comparison of eddy-current loss of a single pole of four damping winding structures

Scheme	Losses by joule effect (W)	
1	851.978	
2	850.707	
3	101.118	
4	13 845.6	

The above chart indicates that when utilizing the solid-steel pole structure, eddy currents create multiple closed-loop paths on the surface of the magnetic poles because they are constructed from a single piece of steel. This results in a substantial increase in rotor pole face eddy-current losses, reaching hundreds of times the losses observed in the other three damping winding configurations. Such strong eddy currents inevitably generate significant additional fields that interact with the main field, dramatically reducing the harmonic content in the no-load magnetic field and creating near-sinusoidal no-load voltage waveforms in the stator windings. However, according to Lenz's Law, this powerful additional field also produces a much stronger demagnetizing effect on the main field than the other three damping winding configurations. Consequently, the no-load voltage induced in the stator windings is significantly lower than that observed with the other three damping winding structures.

To further explore the influence of the additional fields on the characteristics of the no-load voltage waveform, a Fourier decomposition analysis was performed on the measured waveforms. The harmonic components with notable amplitude contributions—including the 5th, 7th, 11th, 13th, and 25th harmonics—are compared in detail, as shown in Fig. 12.

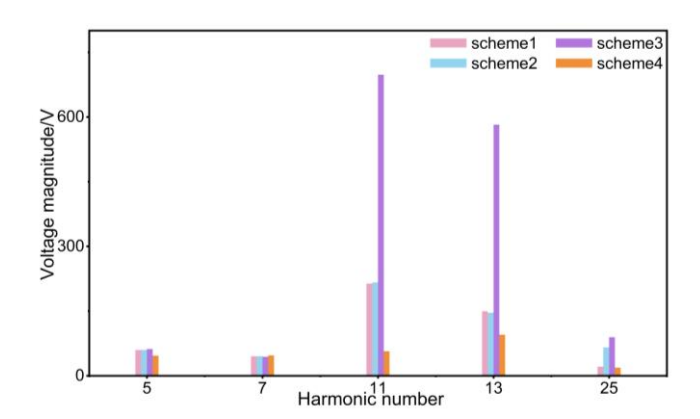


Fig. 12. Comparison of no-load voltage harmonic components of four damping winding structures

As demonstrated in the figure, for harmonic orders of the 5th, 7th, and 25th, the differences in harmonic content among the four damping winding configurations are relatively minimal. However, the impact of their respective additional fields on the 11th and 13th harmonic components of the no-load voltage waveform varies significantly across the configurations. Specifically, when fully damped or semi-damped windings are used, the 11th and 13th harmonic contents exhibit nearly identical levels. In contrast, employing the isolated damping winding structure results in a sharp increase in these harmonic contents. Finally, for the solid-steel pole structure, the harmonic content for both the 11th and 13th harmonics is notably reduced compared to the other three configurations.

4. Computational model validation

To verify the precision of the computational model and its results, we conducted no-load voltage waveform measurements on a specific generator equipped with a fully damped winding configuration. The technical specifications are detailed below.

4.1. Measuring device

The no-load voltage waveform measurements were performed using the instruments listed in Table 6.

Table 6. Instruments required for the no-load voltage waveform measurement test

Equipment	Quantity	Accuracy
8 861 waveform recorder	1	0.2
3 193 digital power meter	1	0.2
FLUKE 187 digital multimeter	2	0.2
10 500 V/100 V potential voltage transformer	3	0.2
10 000 A/150 mV electrical shunt	1	0.2

4.2. Measurement program

The measurement of the no-load voltage waveform is carried out with the connection scheme displayed in Fig. 13.

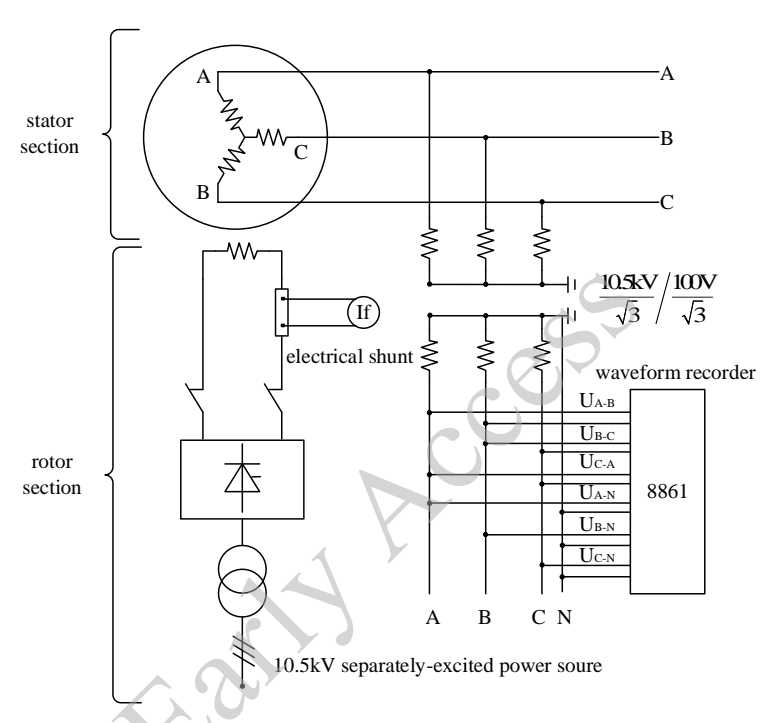


Fig. 13. Connection diagram of the no-load voltage waveform measurement loop

During the testing process, the generator is operated under no-load at its rated voltage and rated speed. The generator stator phase voltages U_{A-N} , U_{B-N} , U_{C-N} , and line voltages U_{A-B} , U_{B-C} , U_{C-A} waveforms are captured using an 8 861-waveform recorder and analyzed through Fourier analysis. Subsequently, the quality parameters of the no-load voltage waveforms, namely THD and THF, are calculated based on Eq. (2), Eq. (3), and the weighting coefficient λ_n of each harmonic content obtained from the "Design and Calculation of Hydro Generator" [1]. These values are recorded as the measured values, which are then compared to the calculated values derived from modeling calculations, as presented in Table 7. Moreover, the harmonics with high magnitudes (250, 350, 550, 650, and 1 250 Hz) are compared, as presented in Table 8, to assess the accuracy of the modeling and computational outcomes.

Table 7. THD, THF validation of the fully damped scheme

	Calculated value	Measured value	Deviation
THD	1.873	1.850	1.243%
THF	1.154	1.186	2.698%

Table 8. Harmonic magnitude validation for the fully damped configuration

	Harmonic magnitude		
Frequency (Hz)	Calculated value	Measured value	
250	59.762	52.631	
350	45.065	41.985	
550	213.695	209.585	
650	149.489	149.678	
1 250	21.214	25.957	

From the test results presented above, it is evident that the calculated values for the no-load voltage waveform quality parameters (THD and THF) and harmonic magnitudes (250, 350, 550 Hz, 650, and 1250 Hz), corresponding to the fully damped configuration, closely align with the measured values, thereby confirming the accuracy and reasonableness of the calculation model used in this study, as well as the reliability of the resulting calculations.

5. Conclusions

The importance of this study lies in establishing a high-precision 2D electromagnetic field finite element model to quantitatively reveal and visually demonstrate the effects of four damping winding structures on no-load magnetic field quality in tubular hydro-generators. This thereby provides direct data support for precision-oriented design and reliability-focused optimization of such generators. The specific findings are outlined as follows:

1. Fully damped and semi-damped structures: The current waveforms and RMS values in the damping windings show minimal differences between fully damped and semi-damped structures. As a result, the additional magnetic fields induced by both configurations have similar effects on the generator's no-load magnetic field. This similarity leads to closely matched results in the respective magnetic field analyses (including field distribution patterns, magnetic flux density, vector magnetic potential magnitude, and air-gap flux density), voltage RMS values, waveforms, THD, THF, and eddy-current losses. Notably, the fully damped structure demonstrates superior quality in the no-load output voltage waveform.

Based on these results, the fully damped configuration is deemed suitable for applications requiring the highest output voltage quality. However, its complete end-ring configuration

substantially raises manufacturing costs and long-term maintenance expenses. Therefore, in scenarios where top voltage waveform quality is not a priority but cost-effectiveness is essential, the semi-damped structure offers a better balance of performance and economics.

2. Isolated damping bar structure: In this configuration, the damping bars are not electrically connected. Eddy currents are limited to individual bars, resulting in significantly weaker bar currents (approaching zero) compared to the entire and semi-damped structures. Consequently, this design yields the lowest eddy-current losses among the four damping schemes. The diminished additional magnetic field generated does not provide significant optimization for the main generator field, resulting in less improvement in the no-load voltage waveform. Notably, there is an increase in the 11th and 13th harmonic content in the no-load voltage, leading to marked fluctuations and producing the lowest waveform quality among all configurations.

While the isolated damping bar structure eliminates the need for end rings and related welding processes/materials, thereby simplifying construction and reducing potential failure points along with manufacturing and maintenance costs, it significantly weakens the capability to suppress stator harmonic field penetration into the rotor. Furthermore, this configuration undermines the rotor's ability to maintain synchronous speed following disturbances. For these reasons, its practical application is not advisable.

3. Solid-steel pole structure: The pole is made from a solid block of steel. Prominent eddy-current paths develop near the surface of the pole, forming several complete closed loops. This phenomenon leads to a significant increase in eddy currents and associated losses. Among the four structures, the additional induced magnetic field has the most significant effect on the generator's no-load field. This extra field likely helps reduce harmonics (particularly the 11th and 13th), thereby optimizing the no-load voltage waveform. Simultaneously, in accordance with Lenz's law, the substantial eddy currents create a counteracting magnetic field that opposes the main field. This results in a notable decrease in the strength of the no-load magnetic field, as indicated by reductions in magnetic flux density, vector magnetic potential magnitude, and airgap flux density amplitude, leading to a lower no-load voltage amplitude.

Moreover, although the solid-steel pole design negates the material costs associated with damping windings and the lamination of poles, meeting the required output voltage amplitude does necessitate an increase in excitation current. This increase raises pole eddy-current losses and significantly heightens the demands on the cooling system, which in turn escalates operational costs. Consequently, solid-steel poles are not advisable for large hydro-generators.

Appendix A

Cross-sectional view of the 2D transient electromagnetic field model

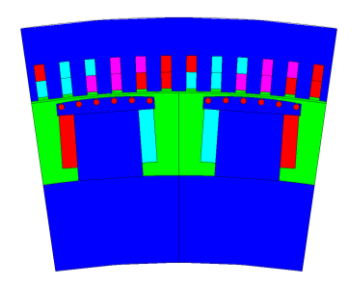


Fig. A1. Cross-sectional view of a two-dimensional transient electromagnetic field model of a pair of magnetic poles

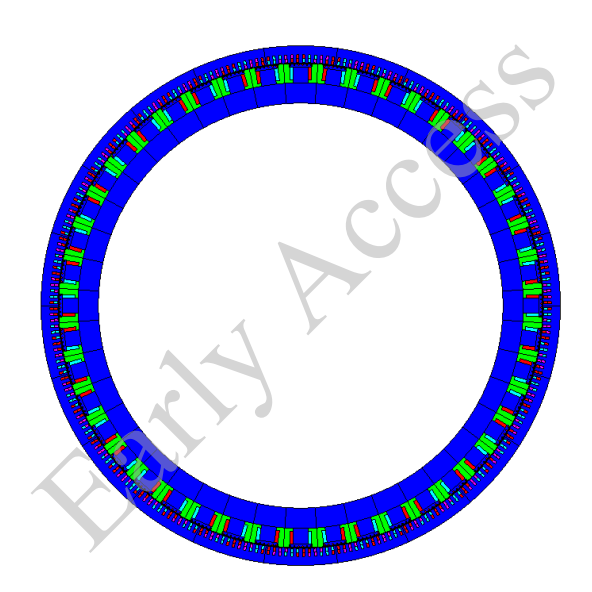


Fig. A2. Cross-sectional view of the 2D transient electromagnetic field model

Appendix B

Structural distribution of stator winding

In the electromagnetic field model, the current flow direction for each winding is as shown in Fig. B1, where "+" denotes current inflow and "-" denotes current outflow. The air gap is located above the stator slots.

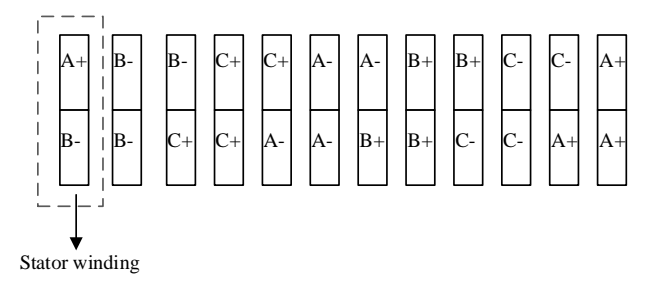


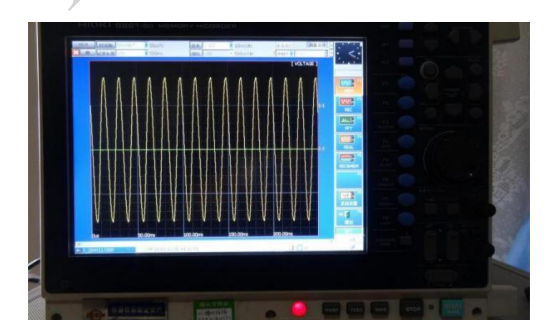
Fig. B1. Structural distribution of stator winding within the electromagnetic field model

Appendix C

No-load voltage test scenes and test waveform



(a) No-load voltage waveform test scene 1



(b) No-load voltage waveform test scene 2

Fig. C1. No-load voltage waveform test scenes

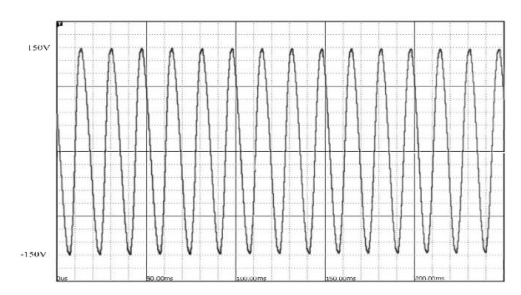


Fig. C2. No-load voltage test waveform of the A–B line voltage (U_{A –B)

References

- [1] Bai Yannian, Design and Calculation of Hydro Generator, Machinery Industry Press (1982).
- [2] Chen Xifang, *Hydraulic Turbine Generator Electromagnetism and Calculation*, China Water Conservancy and Hydropower Press (2011).
- [3] Gu Shifu, Bian Zuying, Zhou Zhiting, Yang Yong, Fan Zhennan, The Disadvantageous Influence and Improvement Measures of Stator Slot Skewed Structures on the Damper Winding Loss and Stator Core Loss of Tubular Hydro-Generators, Journal of Electrical Engineering & Technology, vol. 18, no. 4, pp. 2737–2748 (2022), DOI:10.1007/s42835-022-01333-7.
- [4] Hu Jingming, Gou Zhide, Wang Jiangang et al., Optimization of Voltage Waveform for Variable Speed Generating Motors, Large Electric Machine Technology, vol. 2022, no. 6, pp. 14–20+67 (2022)
- [5] Ni S.J., Bauw G., Romary R., Cassoret B., Le B.J., *Damper Winding for Noise and Vibration Reduction of a Permanent Magnet Synchronous Machine*, Sensors, vol. 22, no. 7, pp. 2738–2738 (2022), DOI:10.3390/s22072738.
- [6] Yin Xi, Zhu Nanlong, Zhu Yifeng, Optimization Analysis of Influencing Factors on No-Load Voltage Waveform of Pumped Storage Motor Based on Taguchi Method, Hydroelectric Power Station Mechanical and Electrical Technology, vol. 45, no. 2, pp. 44–47+128 (2022), DOI: 10.13599/j.cnki.11-5130.2022.02.012.
- [7] Bian Zuying, Zhou Zhiting, Fan Zhennan, No-Load Voltage and Damper Winding Loss and Heat Analysis of the Pole Shoe and Damper Winding Centre Line Shifted Structure of Tubular Hydro-Generators, Electronics Letters, vol. 57, no. 18, pp. 691–693 (2021), DOI:10.1049/ell2.12227.
- [8] Zhen-nan F., Li H., Yong L., Li-dan X., Kun W., Jun W., Effect of Shifting the Pole-shoe and Damper-bar Centerlines on the No-load Voltage Waveform of a Tubular Hydro-generator, Journal of Electrical Engineering & Technology, vol. 13, no. 3, pp. 1294–1303 (2018).
- [9] Fan Zhennan, Han Li, Liao Yong, Suppression of No-Load Voltage Waveform Distortion and Damping Bar Loss Heating in Cross-Flow Hydro Generators, Journal of Electrical Machines and Control, vol. 20, no. 4, pp. 17–26 (2016), DOI:10.15938/j.emc.2016.04.003.
- [10] Zhi-gang Z., Zhen-nan F., No-Load Voltage Waveform Optimization of Integral Number Slots Large Hydro-Generator by Increase the Number of Damper Bars per Pole, Advanced Materials Research, vol. 756-759, pp. 3909–3913 (2013), DOI: 10.4028/www.scientific.net/AMR.756-759.3909.
- [11] Fan Zennan, Liao Yong, Xie Lidan, Zhou Guanghou, Optimization of No-Load Voltage Waveform and Damping Bar Heating Suppression in Axial-Flow Hydro Generators, High Voltage Technology, vol. 38, no. 5, pp. 1233–1242 (2012).
- [12] Zou Hui, Fan Zennan, Research on the Influence of Stator Skewed Slot Design on No-Load Voltage of Axial-Flow Hydro Generators, Hydropower, vol. 38, no. 2, pp. 50–53 (2012).
- [13] Zhang Yujiao, Sun Mengyun, Ruan Jiangjun, Huang Tao, Analysis of No-Load Characteristics and Calculation of Rated Excitation Current of Multiphase Synchronous Generators Based on Finite Element Method, Large Electric Machine Technology, vol. 2012, no. 1, pp. 13–18 (2012).

- [14] Zhou Guanghou, Han Li, Fan Zhennan, *Optimization of No-Load Voltage Waveform of Hydro Generators Using Asymmetric Poles*, Proceedings of the CSEE, vol. 29, no. 15, pp. 67–73 (2009).
- [15] Zhou Guanghou, Zhang Tianpeng, Finite Element Calculation of No-Load Voltage Waveform and Harmonics of Large Hydro Generators, Oriental Electrical Review, vol. 2008, no. 2, pp. 32–37 (2008).
- [16] Keller S., Xuan M.T., Simond J.J., Computation of the No-Load Voltage Waveform of Laminated Salient-Pole Synchronous Generators, IEEE Transactions on Industry Applications, vol. 42, no. 3, pp. 681–687 (2006), DOI:10.1109/TIA.2006.873663.
- [17] Shaogang H., Shanming W., Yonghong X., Calculation of No-Load Voltage Waveform of Synchronous Generators Using Tooth Flux Method, Proceedings of the CSEE, vol. 2005, no. 13, pp. 135–138 (2005).
- [18] Karmaker H., Knight A.M., *Investigation and Simulation of Fields in Large Salient-Pole Synchronous Machines with Skewed Stator Slots*, IEEE Transactions on Energy Conversion, vol. 20, no. 3, pp. 604–610 (2005), DOI:10.1109/TEC.2005.852955.
- [19] Li Huaishu, Li Langru, Rang Yuqi, The Influence of Damping Winding on the No-Load Voltage Waveform of Salient Pole Synchronous Generators, Electric Machines and Control, vol. 2003, no. 4, pp. 267–271 (2003).
- [20] Chen S., *Improvement of Generator Voltage Waveforms—Several Issues of THF*, Small and Medium-sized Electric Machines, vol. 2000, no. 2, pp. 32–36 (2000).
- [21] Liu Chenyu, Determination of Voltage Waveform of Synchronous Generators by Finite Element Magnetic Field Analysis, Small and Medium-sized Electric Machines, vol. 1987, no. 3, pp. 11–15+64 (1987)
- [22] Li Zhesheng, *Measures to Improve the No-Load Voltage Waveform of Salient-Pole Synchronous Generators*, Journal of Harbin University of Electrical Engineering, vol. 1983, no. 3, pp. 1–16 (1983).